Proceedings of the Nineteenth (2009) International Offshore and Polar Engineering Conference
Osaka, Japan, June 21-26, 2009

ISBN 978-1-880653-53-1 (Set); ISSN 1098-618

Hamiltonian Formulation for Water Waves over a Variable Bottom: Asymptotic Models and Numerical Simulations

W. Craig[1], *P. Guyenne*[2] *and C. Sulem*[3]

[1] Department of Mathematics, McMaster University, Hamilton, ON, Canada

[2] Department of Mathematical Sciences, University of Delaware, Newark, DE, USA

[3] Department of Mathematics, University of Toronto, Toronto, ON, Canada

ABSTRACT

We present a Hamiltonian, potential-flow formulation for nonlinear surface water waves in the presence of a variable bottom. This formulation is based on a reduction of the problem to a lower-dimensional system involving boundary variables alone. To accomplish this, we express the Dirichlet–Neumann operator as a Taylor series in terms of the surface and bottom variations. This expansion is convenient for both asymptotic calculations and direct numerical simulations. First, we apply this formulation to the asymptotic description of long waves over random topography. We show that the principal component of the solution can be described as a solution of a Korteweg–de Vries-type equation, plus random phase corrections. We also derive an asymptotic expression for the scattered component. Finally, we propose a pseudospectral method, using the fast Fourier transform, to numerically solve the full equations. Several applications are presented.

KEY WORDS: nonlinear surface waves; long waves; bottom topography; random bottom; Dirichlet–Neumann operator; pseudospectral method.

INTRODUCTION

Because of its relevance to coastal engineering, surface water wave propagation in the presence of an uneven bottom has been studied for many years. The character of coastal wave dynamics can be very complex; waves are strongly affected by the bottom through shoaling and the resulting variations in local linear wave speed, with the subsequent effects of refraction, diffraction and reflection. Nonlinear effects, which influence waves of appreciable steepness even in the simplest of cases, have additional components due to wave-bottom as well as nonlinear wave-wave interactions, as seen, e.g., in depth-induced breaking. The presence of bottom topography in the fluid domain introduces additional space and time scales to the classical perturbation problem. The resulting nonlinear waves can have a great influence on sediment transport and the formation of shoals and sandbars in nearshore regions. It is therefore of central importance to understand the basic mechanisms that govern the dynamics of such waves.

The present paper proposes a new Hamiltonian formulation for surface water waves in the presence of a variable bottom. This formulation lends itself well to asymptotic modeling and analysis, using tools from Hamiltonian perturbation theory, as well as to direct numerical simulations by a pseudospectral method using the fast Fourier transform.

For illustration, we first investigate the problem of long wave propagation over a randomly varying bottom. This problem has drawn serious attention recently with the works of Grataloup and Mei (2003), Nachbin and Sølna (2003), Mei and Li (2004), and Garnier, Muñoz Grajales and Nachbin (2007). Here we adopt a Hamiltonian approach to derive a Korteweg–de Vries-type equation for the principal component of the solution. We also derive an asymptotic expression for the scattered component.

We then present a numerical model that solves the full equations of the problem by a pseudospectral method using the fast Fourier transform. This model is based on an expansion of the Dirichlet–Neumann operator as a Taylor series in terms of the surface and bottom variations, following the idea of Craig and Sulem (1993). See also the works of Dommermuth and Yue (1987), West *et al.* (1987), Liu and Yue (1998), and Smith (1998) for similar methods. Finally, the performance of the model is demonstrated with several applications.

MATHEMATICAL FORMULATION

Governing Equations

We consider the motion of a free surface, $\eta(x,t)$, on top of a fluid domain defined by

$$S(\beta,\eta) = \{(x,y) \in \mathbb{R}^{n-1} \times \mathbb{R} \mid -h+\beta(x) < y < \eta(x,t)\},$$

where $\beta(x)$ denotes the bottom perturbation and $n = 2,3$ is the spatial dimension. The quiescent water level is located at $y = 0$ and the constant reference depth is h. We assume the fluid is incompressible and inviscid, and the flow is irrotational, so that the fluid velocity can be expressed as $u = \nabla\varphi$, where φ denotes the velocity potential. Under the above assumptions, the full boundary value problem for potential flow is given

by

$$\Delta\varphi = 0 \qquad \text{in } S(\beta,\eta)\,, \tag{1a}$$

$$\partial_t\eta + \nabla_x\varphi\cdot\nabla_x\eta - \partial_y\varphi = 0 \qquad \text{at } y=\eta(x,t)\,, \tag{1b}$$

$$\partial_t\varphi + \tfrac{1}{2}|\nabla\varphi|^2 + g\eta = 0 \qquad \text{at } y=\eta(x,t)\,, \tag{1c}$$

$$\nabla\varphi\cdot\nu(\beta) = 0 \qquad \text{at } y=-h+\beta(x)\,, \tag{1d}$$

where g is the acceleration due to gravity, and $\nu(\beta)=(-\nabla_x\beta,1)$ is a (non-normalized) upward vector normal to the bottom. Surface tension effects are neglected but could easily be included in (1c) (see Craig and Nicholls 2000).

Hamiltonian Equations

Following Craig and Sulem (1993), we can reduce the dimensionality of the classical potential flow formulation of the water wave problem, (1), by considering *surface* quantities as unknowns. We begin with the observation that when the free surface $\eta(x,t)$, Dirichlet data at the free surface $\xi(x,t)=\varphi(x,\eta(x,t),t)$ and Neumann data at the bottom $v(x,t)$ are specified, we can in principle solve the full problem, since φ satisfies Laplace's equation with appropriate boundary conditions. In this way, the water wave problem can be reduced from one posed inside the entire fluid domain to one posed at the free surface alone. This fact was originally noted by Zakharov (1968, for deep water), who reformulated (1) as a Hamiltonian system in terms of the canonically conjugate variables η and ξ. In terms of these variables, the equations of motion take the canonical form

$$\partial_t\begin{pmatrix}\eta\\ \xi\end{pmatrix} = \begin{pmatrix}0 & 1\\ -1 & 0\end{pmatrix}\begin{pmatrix}\delta_\eta H\\ \delta_\xi H\end{pmatrix} = J\begin{pmatrix}\delta_\eta H\\ \delta_\xi H\end{pmatrix}\,,$$

or, more specifically,

$$\partial_t\eta = G(\beta,\eta)\xi\,, \tag{2a}$$

$$\begin{aligned}\partial_t\xi = {} & -g\eta - \frac{1}{2(1+|\nabla_x\eta|^2)}\Big[|\nabla_x\xi|^2 - (G(\beta,\eta)\xi)^2\\ & -2(\nabla_x\xi\cdot\nabla_x\eta)G(\beta,\eta)\xi + |\nabla_x\xi|^2|\nabla_x\eta|^2\\ & -(\nabla_x\xi\cdot\nabla_x\eta)^2\Big]\,,\end{aligned} \tag{2b}$$

where H is the Hamiltonian of the system, given by

$$\begin{aligned}H &= \tfrac{1}{2}\int\int_{-h+\beta}^{\eta}|\nabla\varphi|^2\,dy\,dx + \tfrac{1}{2}\int g\eta^2\,dx\,,\\ &= \tfrac{1}{2}\int\xi G(\beta,\eta)\xi\,dx + \tfrac{1}{2}\int g\eta^2\,dx\,,\end{aligned} \tag{3}$$

and $G(\beta,\eta)$ is the so-called Dirichlet–Neumann operator, i.e. the singular integral operator which expresses the normal derivative of the velocity potential on the free surface, in terms of the boundary values ξ and of the domain itself, as parameterized by β and η which define the lower and upper boundaries of the fluid domain. We define this operator by

$$G(\beta,\eta)\,\xi = \nabla\varphi|_{y=\eta}\cdot\nu(\eta)\,,$$

where $\nu(\eta)=(-\nabla_x\eta,1)$ is a (non-normalized) exterior vector normal to the free surface. While this is a linear operator in ξ, it is nonlinear with explicit nonlocal dependence on β and η.

Dirichlet–Neumann Operator

For $\beta=0$, Coifman and Meyer (1985) showed that, if $\eta\in\mathrm{Lip}(\mathbb{R})$, then G is an analytic function of η, from which it follows that G can be written in terms of a convergent Taylor series

$$G(\eta) = \sum_{l=0}^{\infty} G^{(l)}(\eta)\,, \tag{4}$$

where each term $G^{(l)}$ is homogeneous of degree l in η. Craig, Schanz and Sulem (1997) extended these results for periodic $\eta\in C^1(\mathbb{R}^2)$, and Craig and Nicholls (2000) generalized this argument for $\eta\in C^1(\mathbb{R}^{n-1})$. Nicholls and Reitich (2001) devised a direct method to estimate the $G^{(l)}$ (requiring the slightly stronger hypothesis $\eta\in C^{3/2+\delta}(\mathbb{R}^{n-1})$) with the goal of stabilized high-order calculations. A recursion formula for the l-th order term in (4) is given in Craig and Sulem (1993) in two dimensions, and the generalization to three dimensions was derived by Nicholls (1998).

For l odd,

$$\begin{aligned}G^{(l)} = {} & |D|^{l-1}D\frac{\eta^l}{l!}\cdot D - \sum_{j=2,\,\text{even}}^{l-1}|D|^j\frac{\eta^j}{j!}G^{(l-j)}\\ & - \sum_{j=1,\,\text{odd}}^{l}|D|^{j-1}G^{(0)}\frac{\eta^j}{j!}G^{(l-j)}\,,\end{aligned} \tag{5a}$$

and, for $l>0$ even,

$$\begin{aligned}G^{(l)} = {} & |D|^{l-2}G^{(0)}D\frac{\eta^l}{l!}\cdot D - \sum_{j=2,\,\text{even}}^{l}|D|^j\frac{\eta^j}{j!}G^{(l-j)}\\ & - \sum_{j=1,\,\text{odd}}^{l-1}|D|^{j-1}G^{(0)}\frac{\eta^j}{j!}G^{(l-j)}\,,\end{aligned} \tag{5b}$$

where $G^{(0)}=|D|\tanh(h|D|)$, $D=-i\nabla_x$ and $|D|=(-\nabla_x^2)^{1/2}$.

For $\beta\neq 0$, Nicholls and Taber (2008) showed that the Dirichlet–Neumann operator is jointly analytic in all spatial and parametric (boundary) variables, and that it can be analytically continued in the two parametric variables. Craig *et al.* (2005) extended the recursion formulas (5) to the case of an uneven bottom and showed that they can be used verbatim with the exception that the first term $G^{(0)}$ is replaced by

$$G^{(0)} = |D|\tanh(h|D|) + |D|L(\beta)\,. \tag{6}$$

The operator $L(\beta)$, which takes into account the bottom variations, is derived from the Neumann boundary condition at the bottom (1d) and can be expressed as a convergent Taylor series expansion in β,

$$L(\beta) = \sum_{j=0}^{\infty}L_j(\beta)\,,$$

where each term L_j can also be determined explicitly by a recursion formula.

For j odd,

$$\begin{aligned}L_j = {} & -\frac{D}{|D|}\mathrm{sech}(h|D|)\cdot\Big[\frac{\beta^j}{j!}\mathrm{sech}(h|D|)|D|^{j-1}D\\ & + \sum_{l=2,\,\text{even}}^{j-1}\frac{\beta^l}{l!}\cosh(h|D|)|D|^{l-1}DL_{j-l}\\ & - \sum_{l=1,\,\text{odd}}^{j-2}\frac{\beta^l}{l!}\sinh(h|D|)|D|^{l-1}DL_{j-l}\Big]\,,\end{aligned} \tag{7a}$$

and, for $j>0$ even,

$$\begin{aligned}L_j = {} & -\frac{D}{|D|}\mathrm{sech}(h|D|)\cdot\Big[\sum_{l=2,\,\text{even}}^{j-2}\frac{\beta^l}{l!}\cosh(h|D|)|D|^{l-1}DL_{j-l}\\ & - \sum_{l=1,\,\text{odd}}^{j-1}\frac{\beta^l}{l!}\sinh(h|D|)|D|^{l-1}DL_{j-l}\Big]\,.\end{aligned} \tag{7b}$$

For example, the first three terms in the expansion of L are

$$L_0 = 0\,,\quad L_1 = -\frac{D}{|D|}\mathrm{sech}(h|D|)\cdot\beta D\mathrm{sech}(h|D|)\,,$$

$$L_2 = \frac{D}{|D|}\mathrm{sech}(h|D|)\cdot\beta D\sinh(h|D|)L_1\,.$$

It should be noted that multi-valued surfaces (e.g. overturning waves) cannot be described with this formulation.

We next show that this formulation of the water wave problem with a variable bottom is convenient for the derivation of asymptotic models, e.g. for long waves over random topography, as well as for direct numerical simulations of the basic governing equations.

LONG WAVES OVER RANDOM TOPOGRAPHY

Boussinesq and KdV Regimes

Focusing our attention on small-amplitude long waves propagating over a randomly varying bottom, we intend to derive an asymptotic expression for the solution in the Korteweg–de Vries (KdV) scaling regime ($n=2$). As we will show, this consists of a solution of a deterministic KdV-type equation, plus random corrections due to the bottom variations. To do so, we apply successive changes of variables to the Hamiltonian (3) and to the symplectic structure J (Craig, Guyenne and Kalisch 2005), and use scale-separation results (de Bouard *et al.* 2008). The main steps of the procedure are given below.

We assume that the bottom variations β are described by a zero-mean, stationary, ergodic process with mixing properties, and that they take place on length scales shorter than those of the surface waves. This is a question of homogenization theory. Introducing the velocity variable $u=\partial_x\xi$ and using the scaling

$$\varepsilon x = X\,,\;\; u(x)=\varepsilon^2\tilde{u}(X)\,,\;\; \eta(x)=\varepsilon^2\tilde{\eta}(X)\,,\;\; \beta(x)=\varepsilon\tilde{\beta}(X/\varepsilon)\,,$$

where ε is a small parameter, the Hamiltonian can be approximated, up to order $O(\varepsilon^5)$, by

$$H_1=\frac{\varepsilon^3}{2}\int\Big[h_\varepsilon u^2+g\eta^2-\varepsilon^2\Big(\frac{h^3}{3}(\partial_X u)^2-\eta u^2\Big)\Big]dX\,,$$

after dropping the tilde notation. The corrected depth is given by

$$h_\varepsilon = h-\varepsilon\gamma-\varepsilon^2\mathrm{E}(\beta D_x\tanh(hD_x)\beta)\,,$$

where $\gamma(x)=\mathrm{sech}(hD_x)\beta$ and the symbol $\mathrm{E}(.)$ denotes the expected value. The equations of motion then take the form

$$\partial_t\begin{pmatrix}\eta\\ u\end{pmatrix}=\varepsilon^{-3}\begin{pmatrix}0 & -\partial_X\\ -\partial_X & 0\end{pmatrix}\begin{pmatrix}\delta_\eta H_1\\ \delta_u H_1\end{pmatrix}\,,$$

leading to the Boussinesq system

$$\begin{aligned}\partial_t\eta &= -\partial_X\Big[(h_\varepsilon+\varepsilon^2\eta)u\Big]-\varepsilon^2\frac{h^3}{3}\partial_X^3 u\,,\\ \partial_t u &= -g\partial_X\eta-\varepsilon^2 u\partial_X u\,.\end{aligned}$$

The next change of variables is a normal-mode transformation, defined by

$$\eta=\sqrt[4]{\frac{h_\varepsilon}{4g}}(r+s)\,,\quad u=\sqrt[4]{\frac{g}{4h_\varepsilon}}(r-s)=k_\varepsilon(r-s)\,,$$

which reduces the Hamiltonian to

$$\begin{aligned}H_2 &= \frac{\varepsilon^3}{2}\int\Big[\sqrt{gh_\varepsilon}(r^2+s^2)-\frac{\varepsilon^2h^3}{3}\Big(\partial_X(k_\varepsilon r-k_\varepsilon s)\Big)^2\\ &\quad+\frac{\varepsilon^2}{2}k_\varepsilon(r^3-r^2s-rs^2+s^3)\Big]dX\,,\end{aligned}$$

and the equations of motion to

$$\partial_t\begin{pmatrix}r\\ s\end{pmatrix}=J_2\begin{pmatrix}\delta_r H_2\\ \delta_s H_2\end{pmatrix}\,,$$

with

$$J_2=\varepsilon^{-3}\begin{pmatrix}-\partial_X & \frac{1}{4}\frac{\partial_X h_\varepsilon}{h_\varepsilon}\\ -\frac{1}{4}\frac{\partial_X h_\varepsilon}{h_\varepsilon} & \partial_X\end{pmatrix}\,.$$

Finally, the additional scaling $s_1=\varepsilon^{-3/2}s$ puts forward $r(X,t)$ as the main component of the solution which is anticipated to be traveling principally to the right, with a relatively small scattered component $s_1(X,t)$ propagating principally to the left. Accordingly, the evolution equations are rewritten as

$$\partial_t\begin{pmatrix}r\\ s_1\end{pmatrix}=J_3\begin{pmatrix}\delta_r H_3\\ \delta_{s_1} H_3\end{pmatrix}\,, \tag{8}$$

with

$$J_3=\varepsilon^{-3}\begin{pmatrix}-\partial_X & \frac{\varepsilon^{-3/2}}{4}\frac{\partial_X h_\varepsilon}{h_\varepsilon}\\ -\frac{\varepsilon^{-3/2}}{4}\frac{\partial_X h_\varepsilon}{h_\varepsilon} & \partial_X\end{pmatrix}\,,$$

and

$$\begin{aligned}H_3 &= \frac{\varepsilon^3}{2}\int\Big[\sqrt{gh_\varepsilon}(r^2+\varepsilon^3 s_1^2)-\frac{\varepsilon^2h^3}{3}\Big(\partial_X(k_\varepsilon r-\varepsilon^{3/2}k_\varepsilon s_1)\Big)^2\\ &\quad+\frac{\varepsilon^2}{2}k_\varepsilon(r^3-\varepsilon^{3/2}r^2s_1-\varepsilon^3 rs_1^2+\varepsilon^{9/2}s_1^3)\Big]dX\,.\end{aligned}$$

It can be shown that the asymptotic behavior of solutions of (8), as $\varepsilon\to 0$, is governed by the following coupled system of equations

$$\partial_t r = -\partial_X\Big[c_\varepsilon r+\varepsilon^2\Big(c_1\partial_X^2 r+\frac{3}{2}c_2 r^2\Big)\Big]+\varepsilon^2 br\,, \tag{9a}$$

$$\partial_t s_1 = \sqrt{gh}\,\partial_X s_1+\frac{1}{4}\sqrt{\frac{g}{h}}\varepsilon^{-3/2}\partial_x\gamma\Big(\frac{X}{\varepsilon}\Big)r\,, \tag{9b}$$

where the corrected wave speed is

$$c_\varepsilon=\sqrt{gh}\Big(1-\frac{\varepsilon}{2h}\gamma-\varepsilon^2 a_{\mathrm{KdV}}\Big)\,,$$

and

$$\begin{aligned}a_{\mathrm{KdV}} &= \frac{1}{2h}\mathrm{E}(\beta D_x\tanh(hD_x)\beta)+\frac{1}{4h^2}\mathrm{E}(\gamma^2)+\frac{1}{8}\mathrm{E}((\partial_x\gamma)^2)\,,\\ c_1 &= \frac{h^3}{3}\sqrt{\frac{g}{4h}}\,,\quad c_2=\frac{1}{2}\sqrt[4]{\frac{g}{4h}}\,,\\ b &= -\frac{7}{768}\sqrt{\frac{g}{h}}\mathrm{E}((\partial_x\gamma)^3)\,.\end{aligned}$$

Equation (9a) for r has the form of a KdV-type equation, while Eq. (9b) for s_1 is linear with a forcing term by r.

Solution Procedure

We now describe a reduction procedure for system (9) that expresses the solution component $r(X,t)$ in terms of a solution $q(Y,\tau)$ of a deterministic KdV-type equation, under a random change of variables $Y\to X$ and a scaling $\tau=\varepsilon^2 t$ to the KdV time. The scattered component $s_1(X,t)$ has an expression involving integrations along characteristics.

Substitute $r=\partial_X R$ into (9a). The resulting equation for R is

$$\partial_t R=-c_\varepsilon(X)\partial_X R-\varepsilon^2\Big(c_1\partial_X^3 R+\frac{3}{2}c_2(\partial_X R)^2\Big)+\varepsilon^2 bR\,.$$

Transform to characteristic coordinates,

$$\frac{dX}{dt} = c_\varepsilon(X)\ , \quad X(0) = Y\ . \tag{10}$$

Integration of (10) yields

$$X = Y + (1-\varepsilon^2 a_{KdV})t\sqrt{gh} - \frac{\varepsilon^2}{2h}\int_{Y/\varepsilon}^{(Y+t\sqrt{gh})/\varepsilon} \gamma(s)\,ds\ . \tag{11}$$

Then define successively $Q(Y,\tau) = R(X,t)$ and $q(Y,\tau) = \partial_Y Q(Y,\tau)$ so that q satisfies the deterministic equation

$$\partial_\tau q = -c_1\partial_Y^3 q - 3c_2 q\partial_Y q + b\,q\ . \tag{12}$$

If $b = 0$, Eq. (12) is the classical KdV equation. By solving (12) together with the random change of variables $Y \to X$ induced by (10), the solution $r(X,t)$ of (9a) can be expressed as

$$\begin{aligned} r(X,t) &= \partial_X Q = \partial_Y Q\,\partial_X Y \\ &= q(X-\sqrt{gh}t, \varepsilon^2 t) \\ &\quad +\partial_X\Big[q(X-\sqrt{gh}t,\varepsilon^2 t)\Big(\frac{\varepsilon^2}{2h}\int_{(X-\sqrt{gh}t)/\varepsilon}^{X/\varepsilon}\gamma(t')\,dt'\Big)\Big]\ . \end{aligned} \tag{13}$$

By integrating (9b) along left-moving characteristics, the scattered component reads

$$\begin{aligned} s_1(X,t) &= s_1(X+\sqrt{gh}t,0) \\ &\quad +\frac{\varepsilon^{-3/2}}{4h}\int_X^{X+\sqrt{gh}t}\partial_x\gamma\big(\frac{\theta}{\varepsilon}\big)r\big(\theta,t+\frac{X-\theta}{\sqrt{gh}}\big)d\theta\ . \end{aligned} \tag{14}$$

In the limit $\varepsilon \to 0$, the transformation (11) converges as a distribution to

$$X = Y + (1-\varepsilon^2 a_{KdV})t\sqrt{gh} - \frac{\varepsilon^{3/2}}{2h}\sigma_\beta\sqrt[4]{gh}B(t)\ , \tag{15}$$

and expressions (13) and (14) are asymptotic to

$$\begin{aligned} r(X,t) &= q(X-\sqrt{gh}t,\varepsilon^2 t) \\ &\quad +\frac{\varepsilon^{3/2}}{2h}\sigma_\beta\sqrt[4]{gh}\,\partial_X\Big[q(X-\sqrt{gh}t,\varepsilon^2 t)B(t)\Big]\ , \end{aligned} \tag{16}$$

and

$$\begin{aligned} s_1(X,t) &= s_1(X+\sqrt{gh}t,0) \\ &\quad +\frac{1}{4h\sigma_\beta}\int_X^{X+\sqrt{gh}t}B(\theta) \\ &\quad \times\frac{d^2}{d\theta^2}q(2\theta-X-\sqrt{gh}t,\varepsilon^2(t+\frac{X-\theta}{\sqrt{gh}}))d\theta \\ &\quad +\frac{1}{4h\sigma_\beta}\Big[\partial_X B(X+\sqrt{gh}t)q(X+\sqrt{gh}t,0) \\ &\quad -\partial_X B(X)q(X-\sqrt{gh}t,\varepsilon^2 t)\Big] \\ &\quad -\frac{1}{2h\sigma_\beta}\Big[B(X+\sqrt{gh}t)\partial_X q(X+\sqrt{gh}t,0) \\ &\quad -B(X)\partial_X q(X-\sqrt{gh}t,\varepsilon^2 t)\Big]\ , \end{aligned} \tag{17}$$

where σ_β^2 denotes the variance of β and B is Brownian motion.

Further analysis of system (9) together with solutions (16) and (17) is work in progress.

Discussion

(i) Equation (12) contains a linear term which acts as damping or forcing depending on the sign of b. If $b < 0$, solutions decay to zero, while they grow in time if $b > 0$. A sketch of a bottom for which $b < 0$ is shown in Fig. 1.

(ii) If the statistics of β are reversible, meaning that they are preserved under the inversion $x \to -x$, then $\mathrm{E}((\partial_x\beta)^3) = 0$ implying that $b = 0$.

(iii) Equation (16) indicates that coherent wave solutions (e.g. solitary waves) persist, and maintain the same basic properties of momentum and energy transport as in the classical problem of a flat bottom. However, these solutions are modified by two random and realization-dependent effects. First, from (15), the solutions' phase has a random component which, in the asymptotic limit, is governed by Brownian motion. Second, from (16), there is a modulation of the solutions' amplitude by a white noise process (the derivative of Brownian motion). These two manifestations of randomness are correlated. Finally, as shown in (17), the scattered component can be expressed in terms of a diffusion process which is a weighted integral of white noise.

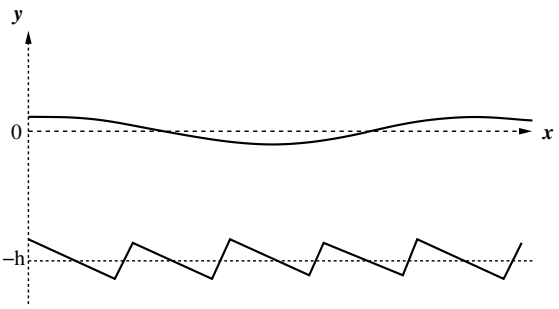

Figure 1: Sketch of a fluid domain with a bottom for which $b < 0$.

DIRECT NUMERICAL SIMULATIONS

Numerical Model

In this section, we present a numerical model that solves the full equations (2) in both two and three space dimensions. We first describe the numerical methods for space and time discretizations of the model, and then show some applications.

Spatial discretization: We assume periodic boundary conditions in the x-direction and use a pseudospectral method. This is a natural choice for the computation of the Dirichlet–Neumann operator, since each term in its Taylor series consists of concatenations of Fourier multipliers (e.g. D and $|D|\tanh(h|D|)$) with powers of β and η.

More specifically, the functions β, η and ξ are represented by truncated Fourier series with the same number of modes N. Applications of Fourier multipliers are performed in Fourier space, while nonlinear products are calculated in physical space at a discrete set of equally spaced points. For example, application of $|D|\tanh(h|D|)$ in physical space is equivalent to multiplication by $|k|\tanh(h|k|)$ in Fourier space (where k denotes the wavenumber). All these operations can be performed efficiently by using the fast Fourier transform.

Both operators G and L are also approximated by a finite number of terms,

$$G(\beta,\eta) \simeq \sum_{l=0}^{M} G^{(l)}(\beta,\eta)\ , \quad L(\beta) \simeq \sum_{j=0}^{M_b} L_j(\beta)\ ,$$

where M and M_b are chosen according to the physical problem under

consideration. In practice, it is not necessary to specify large values for M and M_b (typically $M, M_b < 10$) since the series converge rapidly owing to the analyticity properties of the Dirichlet–Neumann operator.

Note that there are no *a priori* restrictions on the relative length scales between bottom and surface variations. In particular, the method is not restricted to slowly varying topography compared to surface waves. However, because of the character of Taylor series expansions and the use of fast Fourier transforms, bottom and surface variations are both required to be single-valued, sufficiently smooth and of moderate amplitude.

Time integration: Time integration is carried out in Fourier space. The linear terms in (2) are solved exactly by an integrating factor technique. The nonlinear terms are integrated in time using a fourth-order Runge–Kutta scheme with constant step size.

In the computations (especially of large-amplitude waves), it was observed that spurious oscillations can develop in the wave profile, due to the onset of an instability related to the growth of numerical errors at high wavenumbers. Similar instabilities were observed by other authors (Dommermuth and Yue 1987) who used smoothing techniques to circumvent this difficulty. Here, at every time step, we apply an ideal low-pass filter to both η and ξ, of the form

$$\gamma_k = \begin{cases} 1 & \text{if} \quad |k|/k_{\max} \le \theta\,, \quad 0 < \theta \le 1\,, \\ 0 & \text{if} \quad |k|/k_{\max} > \theta\,, \end{cases}$$

where $k_{\max}$ is the largest wavenumber of the spectrum. Typically, we found that $\theta = 0.8$ suffices to stabilize the solution. Care is taken to specify a sufficiently high spatial resolution and a value of θ close to unity so that only energy levels located in the high-wavenumber region of the spectrum are suppressed by filtering. In most of our simulations with small to moderate amplitudes (e.g. Bragg reflection over sinusoidally varying topography, harmonic generation over a submerged bar; see below), no filtering was used at all.

Further details on the numerical methods, together with numerical tests, are given in Guyenne and Nicholls (2005, 2007).

Numerical Results

Here we show two-dimensional ($n = 2$) simulations to illustrate the performance of the numerical model. Comparisons with experimental data and other numerical models are provided. Unless stated otherwise, all variables are non-dimensionalized according to long-wave theory, i.e, lengths are divided by h and times divided by $\sqrt{h/g}$.

Solitary wave shoaling on slope: The first experiment concerns the evolution of solitary waves traveling up a plane slope, and our computations are compared with results obtained by a boundary element method (Grilli *et al.* 2001; Guyenne and Grilli 2006). The bottom geometry is depicted in Fig. 2; the initial condition is a fully nonlinear solitary wave of amplitude a_0 computed by Tanaka's method (Tanaka 1986). Because reflecting lateral boundaries are used in the boundary element code, both the bottom geometry and initial condition in the present model are specified symmetrically about the center of the domain in order to simulate a reflecting boundary condition at some distance up the slope. As shown in Fig. 2, the situation is two solitary waves propagating symmetrically towards a submerged island between them.

We present results for two simulations with incident solitary waves of amplitudes $a_0 = 0.3, 0.4$. In both cases, the bottom slope is fairly steep ($s = 1/18$). We used $M = 8$, $M_b = 4$ and $N = 512$. Figures 3–4 show a comparison of wave profiles at two advanced stages of shoaling. The boundary element solution exhibits a slightly sharper and higher wave crest than the spectral solution, and these discrepancies become more pronounced as the solitary waves approach breaking. Nevertheless, the overall agreement is good. The rear faces of the waves match almost perfectly and the wave crests have nearly the same locations.

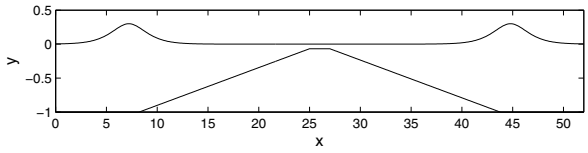

Figure 2: Bottom topography and initial condition in the solitary wave shoaling problem. The two solitary waves are of amplitude $a_0 = 0.3$ and the bottom slope is $s = 1/18$.

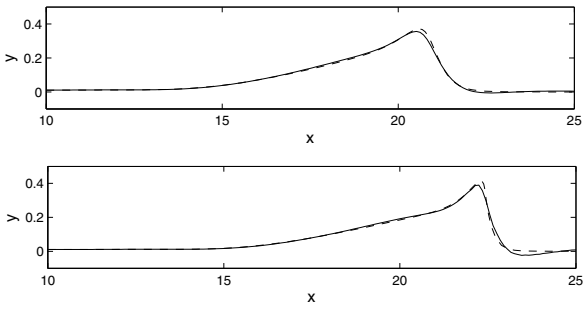

Figure 3: Comparison of solitary wave profiles between boundary element (dashed line) and spectral (solid line) methods, for $a_0 = 0.3$ at times (a) $t = 12$ and (b) $t = 13.6$.

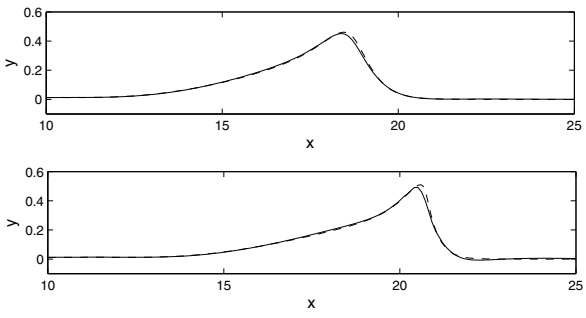

Figure 4: Comparison of solitary wave profiles between boundary element (dashed line) and spectral (solid line) methods, for $a_0 = 0.4$ at times (a) $t = 10.2$ and (b) $t = 12$.

Bragg reflection over sinusoidally varying topography: We now consider Bragg reflection over a sinusoidal ripple patch. For small incident wave and bottom slopes, reflection near Bragg resonance is predicted well by multiple-scale linearized perturbation theory (Mei 1985). Here we numerically examine higher-order nonlinear effects using our spectral model. The conditions in Davis and Heathershaw (1984) are used in order to compare with their experiments. The ripple patch is defined by

$$\beta(x) = d\,\sin(k_b x)\,, \quad -L_b \le x \le L_b\,,$$

as depicted in Fig. 5. The ripple slope is $k_b d = 0.31$, the ripple amplitude is $d = 0.16$, and $L_b/\lambda_b = 10$ (i.e. a patch of 10 sinusoidal ripples, with $\lambda_b = 2\pi/k_b$).

Figure 6 shows the computed reflection coefficient for incident waves of steepness $ka_0 = 0.05$ and wavenumber k near the linear Bragg resonance condition $2k/k_b = 1$ ($M = M_b = 2$ and $N = 512$). We used the least-squares method of Mansard and Funke (1990) to evaluate the reflection coefficient from time series in the steady state. For comparison, experimental data by Davis and Heathershaw (1984) along with the linear solution by Mei (1985) are also plotted in Fig. 6. We observe a downshift of the resonant peak relative to the linear value, in accordance with the experimental data. This wavenumber downshift is not predicted by linear theory and can be attributed to nonlinear effects, as reported by other authors (Liu and Yue 1998).

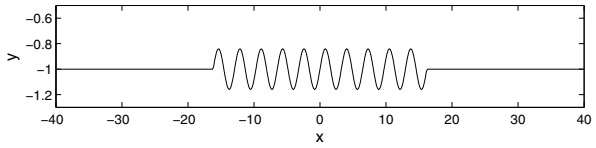

Figure 5: Bottom topography with a patch of 10 sinusoidal ripples of amplitude $d = 0.16$ and slope $k_b d = 0.31$.

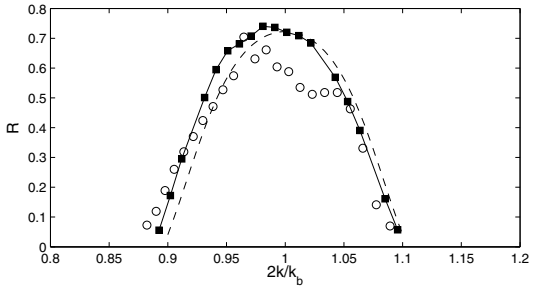

Figure 6: Bragg reflection coefficient near the linear resonance condition $2k/k_b = 1$, for $ka_0 = 0.05$, $k_b d = 0.31$, $d = 0.16$: experiments (circles), linear theory (dashed line), and our numerical simulations (squares-solid line).

Harmonic generation over a submerged bar: It is well-known that regular waves decompose into higher-frequency free waves as they propagate past a submerged bar, as shown in experimental work (Dingemans 1994). As the waves travel up the front slope of the bar, higher harmonics are generated due to nonlinear interactions, causing the waves to steepen. These harmonics are then released as free waves on the downslope, producing an irregular pattern behind the bar. Here we compare our spectral model with experimental data of Dingemans (1994). The geometry of the submerged bar is illustrated in Fig. 7.

We present numerical results for two different incident wave conditions: $(T_0, a_0) = (2.02\,\mathrm{s}, 0.02\,\mathrm{m})$ and $(2.525\,\mathrm{s}, 0.029\,\mathrm{m})$, where T_0 and a_0 denote the incident wave period and height, respectively. Time histories of the surface elevation at various locations are shown in Figs. 8–9. In both cases, the computations were performed using $M = M_b = 8$ and $N = 2048$. The time origin was shifted so that the numerical results match the measurements for the first wave gauge at $x = 2\,\mathrm{m}$. Overall, the computations compare well with the experimental data in both cases. In particular, the asymmetry of the shoaling waves and the generation of higher harmonics are reproduced well by the numerical model. Note that, in the second case (which corresponds to an incident wave of larger amplitude than in the first case), some discrepancies are observed for gauges downstream from the top of the bar (i.e. $x > 13.5\,\mathrm{m}$). This may be explained by the occurrence of spilling breakers in the experiments as reported in Dingemans (1994) for this case.

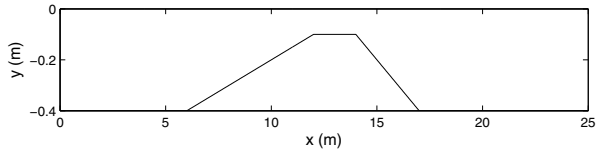

Figure 7: Submerged bar for harmonic wave generation as described in the experiments of Dingemans (1994).

CONCLUSIONS

We have presented a Hamiltonian formulation for nonlinear surface water waves in the presence of a variable bottom. This formulation is convenient for both asymptotic calculations and direct numerical simulations. First, we have applied this formulation to the asymptotic description of long waves over random topography. We have shown that the principal component of the solution can be described as a solution of a KdV-type equation, plus random phase corrections. We have also derived an asymptotic expression for the scattered component. Finally, we have proposed a spectral method, based on this Hamiltonian formulation, to numerically solve the full equations of the problem. Several applications have been shown to demonstrate its performance.

ACKNOWLEDGEMENTS

W. Craig acknowledges support by the Canada Research Chairs Program and NSERC through grant number 238452-01, P. Guyenne acknowledges support by the University of Delaware Research Foundation and NSF through grant number DMS-0625931, and C. Sulem acknowledges support by NSERC through grant number 46179-05.

REFERENCES

de Bouard, A., Craig, W., Díaz-Espinosa, O., Guyenne, P. and C., Sulem (2008). "Long wave expansions for water waves over random topography," *Nonlinearity*, Vol 21, pp. 2143-2178.

Coifman, R. and Y., Meyer (1985). "Nonlinear harmonic analysis and analytic dependence," *Pseudodifferential Operators and Applications*, AMS, Providence, RI, pp. 71-78.

Craig, W., Guyenne, P. and H., Kalisch (2005). "Hamiltonian long wave expansions for free surfaces and interfaces," *Comm. Pure Appl. Math.*, Vol 58, pp. 1587-1641.

Craig, W., Guyenne, P., Nicholls, D.P. and C., Sulem (2005). "Hamiltonian long wave expansions for water waves over a rough bottom," *Proc. R. Soc. Lond. Ser. A Math. Phys. Eng. Sci.*, Vol 461, pp. 839-873.

Craig, W. and D.P., Nicholls (2000). "Traveling two and three dimensional capillary gravity water waves," *SIAM J. Math. Anal.*, Vol 32, pp. 323-359.

Craig, W., Schanz, U. and C., Sulem (1997). "The modulation regime of three-dimensional water waves and the Davey–Stewartson system," *Ann. Inst. Henri Poincaré Anal. Non Linéaire*, Vol 14, pp. 615–667.

Craig, W. and C., Sulem (1993). "Numerical simulation of gravity waves," *J. Comp. Phys.*, Vol 108, pp. 73-83.

Davis, A.G. and A.D., Heathershaw (1984). "Surface wave propagation over sinusoidally varying topography," *J.Fluid Mech.*, Vol 144, pp. 419-443.

Dingemans, M.W. (1994). "Comparison of computations with Boussinesq-like models and laboratory measurements," *Technical report H1684.12*, Delft Hydraulics, The Netherlands.

Dommermuth, D.G. and D.K.P., Yue (1987). "A high-order spectral method for the study of nonlinear gravity waves," *J. Fluid Mech.*, Vol 184, pp. 267-288.

Garnier, J., Muñoz Grajales, J.C. and A., Nachbin (2007). "Effective behavior of solitary waves over random topography," *Multiscale Modeling Simul.*, Vol 6, pp. 995-1025.

Grataloup, G and C.C., Mei (2003). "Long waves in shallow water over a random seabed," *Phys. Rev E*, Vol 68, 026314.

Grilli, S.T., Guyenne, P. and F., Dias (2001). "A fully nonlinear model for three-dimensional overturning waves over an arbitrary bottom," *Int. J. Numer. Meth. Fluids*, Vol 35, pp. 829-867.

Guyenne, P. and S.T., Grilli (2006). "Numerical study of three-dimensional overturning waves in shallow water," *J. Fluid Mech.*, Vol 547, pp. 361-388.

Guyenne, P. and D.P., Nicholls (2005). "Numerical simulation of solitary waves on plane slopes," *Math. Comp. Simulation*, Vol 69, pp. 269-281.

Guyenne, P. and D.P., Nicholls (2007). "A high-order spectral method for nonlinear water waves over moving bottom topography," *SIAM J. Sci. Comp.*, Vol 30, pp. 81-101.

Liu, Y. and D.K.P., Yue (1998). "On generalized Bragg scattering of surface waves by bottom ripples," *J. Fluid Mech.*, Vol 356, pp. 297-326.

Mansard, E.P.D. and E.R., Funke (1980). "The measurement of incident and reflected spectra using a least squares method," *Proc. 17th Coastal Engng Conf.*, New York, USA, pp. 154-172, ASCE.

Mei, C.C. (1985). "Resonant reflection of surface water waves by periodic sandbars," *J. Fluid Mech.*, Vol 152, pp. 315-335.

Mei, C.C. and Y., Li (2004). "Evolution of solitons over a randomly rough seabed," *Phys. Rev. E*, Vol 70, 016302.

Nachbin, A. and K., Sølna (2003). "Apparent diffusion due to topographic microstructure in shallow waters," *Phys. Fluids*, Vol 15, pp. 66-77.

Nicholls, D.P. (1998). "Traveling water waves: Spectral continuation methods with parallel implementation," *J. Comp. Phys.*, Vol 143, pp. 224-240.

Nicholls, D.P. and F., Reitich (2001). "A new approach to analyticity of Dirichlet–Neumann operators," *Proc. R. Soc. Edinburgh Sect. A*, Vol 131, pp. 1411-1433.

Nicholls, D.P. and M., Taber (2008). "Joint analyticity and analytic continuation of Dirichlet–Neumann operators on doubly perturbed domains," *J. Math. Fluid Mech.*, Vol 10, pp. 238-271.

Smith, R.A. (1998). "An operator expansion formalism for nonlinear surface waves over variable depth," *J. Fluid Mech.*, Vol 363, pp. 333-347.

Tanaka, M. (1986). "The stability of solitary waves," *Phys. Fluids*, Vol 29, pp. 650-655.

West, B.J., Brueckner, K.A., Janda, R.S., Milder, D.M. and R.L., Milton (1987). "A new numerical method for surface hydrodynamics," *J. Geophys. Res.*, Vol 92, pp. 11803-11824.

Zakharov, V.E. (1968). "Stability of periodic waves of finite amplitude on the surface of a deep fluid," *J. Appl. Mech. Tech. Phys.*, Vol 9, pp. 190-194.

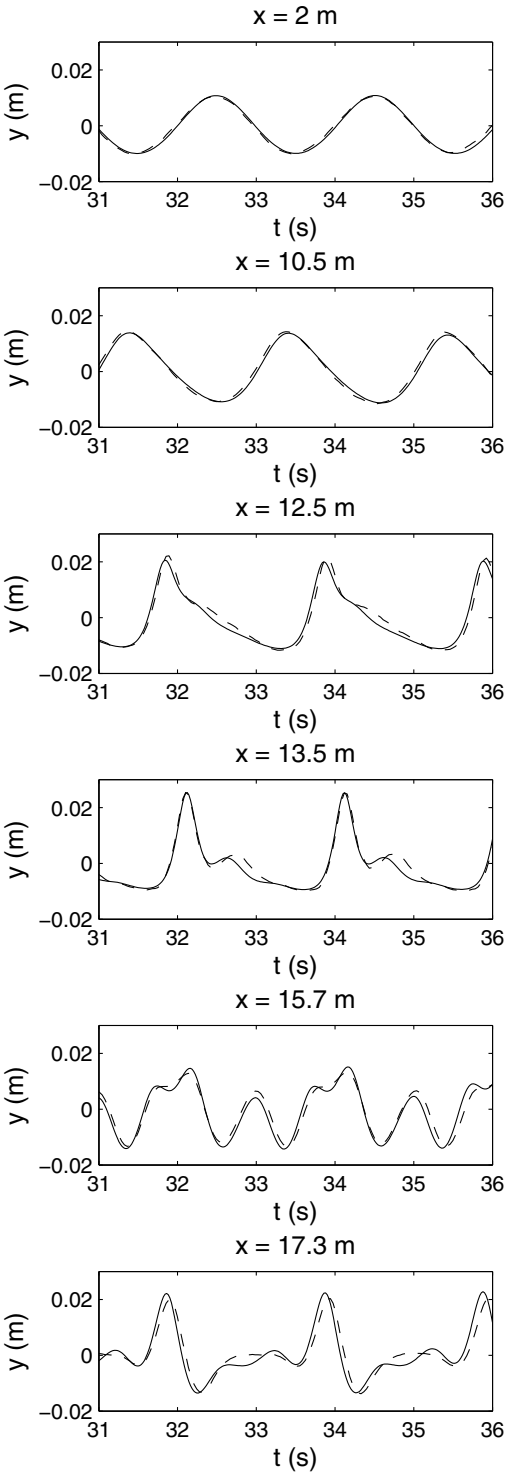

Figure 8: Time series of surface elevations at various locations for waves passing over a bar: experiments (dashed line) and numerical simulations (solid line): $T_0 = 2.02$ s and $a_0 = 0.02$ m.

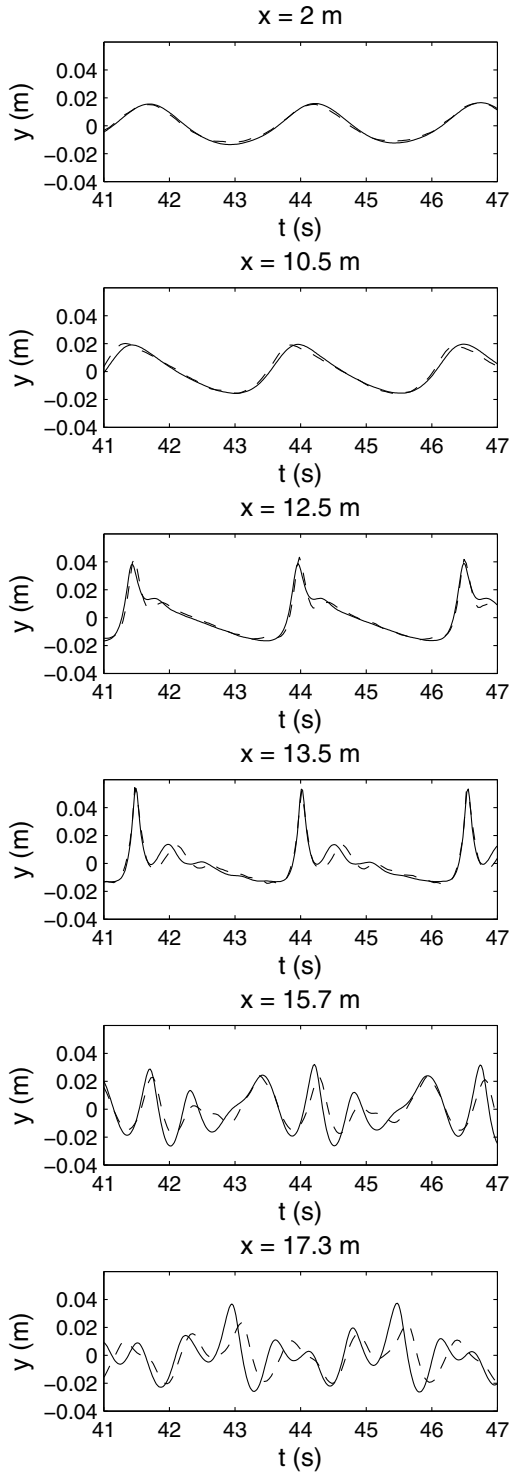

Figure 9: Time series of surface elevations at various locations for waves passing over a bar: experiments (dashed line) and numerical simulations (solid line): $T_0 = 2.525$ s and $a_0 = 0.029$ m.